PCCP

PAPER

View Article Online
View Journal | View Issue

Cite this: *Phys. Chem. Chem. Phys.*, 2025, **27**, 1310

Characterisation of the electronic ground states of BaH^+ and BaD^+ by high-resolution photoelectron spectroscopy

J. R. Schmitz and F. Merkt *

Received 12th November 2024,
Accepted 3rd December 2024

DOI: 10.1039/d4cp04323e

rsc.li/pccp

The rovibrational energy-level structures of BaH^+ and BaD^+ in their $X^+\ ^1\Sigma^+$ electronic ground state have been characterised by pulsed-field-ionisation zero-kinetic-energy photoelectron spectroscopy following resonance-enhanced (1 + 1′) two-photon excitation from the BaH/BaD X $^2\Sigma^+$ ground state *via* the E $^2\Pi_{1/2}$ (v' = 0, 1) intermediate levels. A full set of rovibrational molecular constants for the BaH^+ and BaD^+ ground states has been derived for the first time and the adiabatic ionisation energies of BaH and BaD were determined to be 38 679.96(20) and 38 652.69(20) cm^{-1}, respectively. Photoelectron spectra recorded *via* E-state levels of selected rovibronic parity exhibit pronounced intensity alternations of transitions to rotational states of the cations with even- and odd-valued rotational-angular-momentum quantum number N^+. This observation is interpreted by invoking dominant contributions of even-ℓ photoelectron partial waves in the photoionisation of the E $^2\Pi_{1/2}$ (v' = 0, 1) intermediate states of barium hydride. The lowest pure-rotational transition frequencies of BaH^+ and BaD^+ are derived from the photoelectron spectra which may help the detection of BaH^+ in the microwave and millimetre-wave ranges.

1. Introduction

Alkaline-earth metal hydrides (MH, with M = Be, Mg, Ca, Sr, Ba, Ra) and their singly-charged cations (MH^+) are important diatomic molecules. The lighter species, and in particular $MgH^{(+)}$ and $CaH^{(+)}$, are present in different astrophysical environments, notably near sunspots (see, *e.g.*, ref. 1) and dwarf stars (see, *e.g.*, ref. 2). CaH and BaH belong to the so far still limited category of molecules that can be laser cooled.[3–5] Several of these hydrides and related molecules have been proposed as candidates for the search for physics beyond the standard model of particle physics (see, *e.g.* ref. 6 and 7), to measure the electron electric-dipole moment (eEDM)[8] and the proton-to-electron mass ratio.[9] Cold MgH^+ (ref. 10) and CaH^+ (ref. 11) produced by sympathetic cooling in laser-cooled ion traps have also been studied by high-resolution spectroscopy, and similar experiments on BaH^+ have been proposed in the context of sources of ultracold hydrogen atoms.[12]

MH and MH^+ molecules are also interesting from an electronic-structure point of view. M and M^+ have low-lying excited electronic states and, consequently, MH and MH^+ have numerous low-lying electronic states associated with the different M + H and M^+ + H dissociation asymptotes. Their spectra in the visible range are rich, difficult to analyse, and challenging to calculate accurately from first principles. In the past, they served as benchmark systems for calculations employing effective core potentials, the results of which can then be compared to those obtained from all-electron calculations.[13–15] More recent calculations focus on electronically excited states and their multiconfigurational nature[16–18] with a dedicated effort towards achieving high accuracy to assist laser-cooling applications.[18–21]

The electronic structure of neutral BaH has been thoroughly characterised. The first spectroscopic studies of BaH were performed by Schaafsma[22] and Fredrickson *et al.*[23] who characterised Franck–Condon-diagonal E $^2\Pi_\Omega \rightarrow$ X $^2\Sigma^+$ (v'–v'') red emission bands. Following these studies, Watson[24,25] reported several bands from the A $^2\Pi \rightarrow$ X $^2\Sigma^+$ and B $^2\Sigma^+ \rightarrow$ X $^2\Sigma^+$ emission systems. Later work concentrated on the characterisation of higher-lying electronic states of BaH up to nearly 33 000 cm^{-1} above the ground X $^2\Sigma^+$ (v = 0) level,[26–31] primarily under high-temperature conditions. High-resolution spectroscopic investigations have been conducted on transitions involving the ground X $^2\Sigma^+$ and the first four low-lying H $^2\Delta$, A $^2\Pi$, B $^2\Sigma^+$ and E $^2\Pi_\Omega$ excited states.[30,32–35] Rovibrational transitions in the X $^2\Sigma^+$ state have also been recorded at high-resolution in multiple Ba^1H isotopomers using diode laser spectroscopy[36] and Fourier-transform emission spectroscopy,[37] resulting in the determination of high-precision molecular constants. Ram *et al.*[35] characterised the Franck–Condon-diagonal E $^2\Pi_\Omega$–X $^2\Sigma^+$ (Δv = 0) bands with v' = v'' = 0, 1 and 2 by Fourier-transform emission spectroscopy and were able to improve the values of the molecular constants of the E $^2\Pi_\Omega$ and X $^2\Sigma^+$ states to their current values. In recent work at

Institute of Molecular Physical Sciences, ETH Zurich, CH-8093 Zurich, Switzerland

highest resolution, Zelevinsky and coworkers[20,38,39] investigated the hyperfine structure of the B $^2\Sigma^+$–X $^2\Sigma^+$ and A $^2\Pi_{1/2}$–X $^2\Sigma^+$ band systems and determined vibrational branching ratios in order to find suitable transitions for laser-cooling applications. These investigations culminated in the demonstration of laser cooling in BaH.[4]

In contrast to BaH, hardly any experimental information is available on BaH^+ and the current knowledge of the spectroscopic properties of this cation stems from *ab initio* quantum-chemical investigations. Dos Santos *et al.*[40] have predicted the adiabatic ionisation energy of BaH^+, corresponding to the BaH^+ $X^+\,^1\Sigma^+$ ($v^+ = 0$) ← BaH X $^2\Sigma^+$ ($v'' = 0$) ionisation threshold, to be 4.6627 eV (37 607 cm^{-1}). *Ab initio* quantum-chemical calculations have shown that the $X^+\,^1\Sigma^+$ electronic ground state of BaH^+ is correlated to the $Ba^+(6s)$ + H(1s) dissociation limit and is strongly bound, with a dissociation energy of about 20 000 cm^{-1}.[17,41–43] Aymar *et al.*,[44] Mejrissi *et al.*[42] and Abu el kehr *et al.*[43] have calculated potential-energy functions for many electronic states of BaH^+ up to the $Ba^+(8s)$ + H(1s) dissociation limit, and it is possible, from the potential-energy curves they reported, to see how Rydberg character emerges in the electronically excited states as the excitation energy approaches the BaH^{2+} ionisation threshold.

Our own interest in the heavier members of the MH/MH^+ family originates from the fact that the doubly charged cations MH^{2+} with M = Ca, Sr and Ba are expected to be thermodynamically stable because the ionisation energy of H is larger than those of Ca^+, Sr^+ and Ba^+.[45–47] Moreover, the ionisation energies of MH^+ are low so that their photoelectron spectra can be recorded with table-top laser systems. The Rydberg states of MH^+ are also expected to be stable, with easily resolvable rotational structures. So far, hardly any high-resolution experimental information is available on the structure of doubly-charged molecular cations and on the Rydberg states of singly-charged cations. We hope to fill this gap in the future, following first successes in our investigation of $MgAr^{2+}$.[48]

We report here on the first spectroscopic characterisation of the $X^+\,^1\Sigma^+$ ground electronic states of BaH^+ and BaD^+ using pulsed-field-ionisation zero-kinetic-energy photoelectron (PFI-ZEKE-PE) spectroscopy in combination with the resonant (1 + 1′) two-photon excitation scheme *via* the E $^2\Pi_{1/2}$ intermediate state presented in Fig. 1. This study provides the first stepping stone towards characterising the Rydberg states of BaH^+ and the doubly charged BaH^{2+} molecule.

PFI-ZEKE-PE spectroscopy is a powerful tool for the characterisation of the structure of gas-phase cations:[49–51] it enables spectral resolution sufficient to fully resolve the rotational structure in the photoelectron spectra of diatomic molecules and, unlike pure-rotational and vibrational spectroscopy, it provides access to a very broad range of rovibronic states of the cation. It also reveals the dynamics of the photoionisation process and offers the possibility to prepare molecular ions in specific quantum states. These advantages represent key aspects of our long-term approach to studying singly and doubly charged molecular cations.

2. Experimental setup and procedure

The experimental setup used for this work is shown schematically in Fig. 2. It has been previously described in ref. 52–56 and only the main aspects are repeated here. BaH and BaD were produced in the gas phase by coupling laser-ablation and supersonic-expansion techniques. The frequency-doubled output of a pulsed Nd:YAG laser (wavelength 532 nm, repetition rate 25 Hz, pulse length ≈ 8 ns) was used to ablate barium (Ba) atoms off a rotating Ba rod. BaH or BaD molecules were generated by expanding the vaporised Ba in a H_2/He (1 : 10) and a D_2/He (1 : 10) supersonic jet, respectively, using a pulsed valve. Approximately 25 cm downstream from the valve orifice, the supersonic expansion passed through a 3-mm-diameter skimmer serving the purpose of reducing the transverse velocity of the molecular jet. A small (≤ 50 V) electric potential was applied to the skimmer to prevent ions created in the ablation process from reaching the photoexcitation chamber. After passing through the skimmer, the beam entered a resistively coupled 5.8-cm-long cylindrical electrode stack consisting of five equally spaced electrodes inside the magnetically shielded photoexcitation chamber. This electrode stack served the

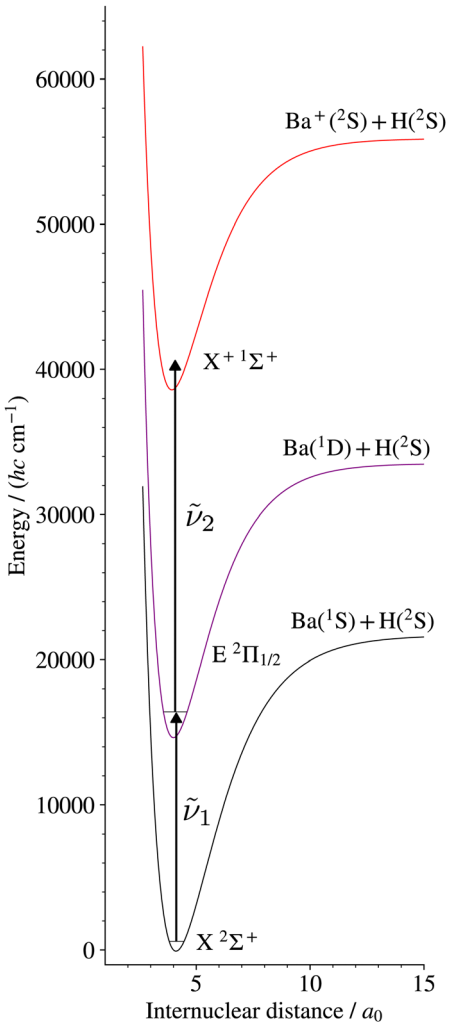

Fig. 1 Resonant multiphoton excitation scheme used to access the $X^+\,^1\Sigma^+$ ground state of BaH^+ from the BaH X $^2\Sigma^+$ ground state. The potential-energy curves are taken from ref. 18 and 44. An analogous excitation scheme was used in BaD to access the BaD^+ ground state.

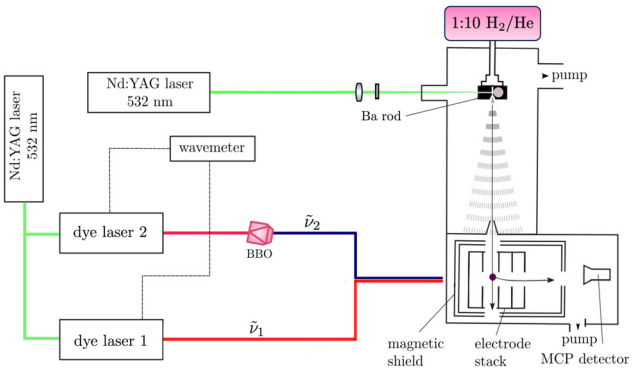

Fig. 2 Schematic representation of the experimental setup used to record (1 + 1′) R2PI and PFI-ZEKE-PE spectra of BaH and BaD. Ba atoms are generated in the gas-phase by laser ablation off a Ba rod. BaH and BaD molecules are formed through reactions with H_2 and D_2, respectively, and entrained in supersonic expansions of H_2/He (1 : 10, volume ratio) and D_2/He (1 : 10). The supersonic beam passes through a skimmer before entering an electrode stack where the molecules are photoexcited using two Nd:YAG-pumped dye lasers from the X $^2\Sigma^+$ ground state to the region of the first ionisation thresholds in a two-photon excitation sequence *via* selected rovibrational levels of the E $^2\Pi_{1/2}$ intermediate state. The output of the second dye laser is frequency-doubled in a BBO crystal. BaH^+ or BaD^+ cations produced by (1 + 1′) R2PI or photoelectrons resulting from pulsed-field ionisation are extracted by applying pulsed electric potentials across the electrode stack and monitored at a microchannel-plate (MCP) detector located at the end of a time-of-flight (TOF) tube.

purpose of applying electric-field pulses to field ionise high Rydberg states produced by photoexcitation and extract the electrons, or ions, for detection.

To access the low-lying states of BaH^+ and BaD^+, BaH and BaD were photoexcited from the ground X $^2\Sigma^+$ ($v'' = 0$) state in a two-colour, two-photon process *via* the intermediate E $^2\Pi_{1/2}$ ($v' = 1$, 0) states, which were accessed using the output of a Nd:YAG-pumped dye laser of wavenumber $\tilde{\nu}_1$. These intermediate states were specifically selected for the large Franck–Condon factors and the large electric-dipole transition moments from the X $^2\Sigma^+$ ($v'' = 0$) state. To avoid saturation and line broadening, the energy of the photoexcitation pulse was reduced to below 20 μJ. To either ionise BaH/BaD in (1 + 1′) resonance-enhanced two-photon ionisation (R2PI) experiments or to excite BaD/BaH to high-lying Rydberg states in the PFI-ZEKE-PE measurements, the output of a second Nd:YAG-pumped dye laser of frequency ν_2 was employed, which was frequency-doubled (pulse length ∼8 ns, bandwidth ≈ 0.15 cm^{-1}) using a beta-barium-borate (BBO) crystal. The pulsed laser beams ($\tilde{\nu}_1$ and $\tilde{\nu}_2$) were spatially overlapped before entering the photoexcitation chamber, where they crossed the molecular beam at right angles. The fundamental wavenumbers of both dye lasers were calibrated using a wavemeter with a specified accuracy of 0.02 cm^{-1}. The pulses from the second laser were delayed by ∼5 ns with respect to those of the first laser to minimise contributions to the ion signal from nonresonant ionisation processes.

In the (1 + 1′) R2PI measurements, a pulsed electric field of +172 V cm^{-1} was applied across the electrode stack to extract the BaH^+/BaD^+ cations for mass-selective detection at a microchannel-plate (MCP) detector located at the end of a 15-cm-long linear time-of-flight (TOF) mass spectrometer. (1 + 1′) R2PI spectra were measured by monitoring the BaH^+ or BaD^+ ion signal as a function of the wavenumber $\tilde{\nu}_1$ of the first laser. $^{134}BaH^+$, $^{135}BaH^+$, $^{136}BaH^+$, $^{137}BaH^+$ and $^{138}BaH^+$, with 0.02417(18), 0.06592(12), 0.07854(24), 0.11232(24), and 0.71698(42) natural abundances,[57] respectively, were resolved in the TOF spectra and their (1 + 1′) R2PI spectra recorded separately. Only the ^{138}BaH (and ^{138}BaD) (1 + 1′) R2PI spectra were analysed because the $^A BaH^+$ ($^A BaD^+$) ion times of flight overlapped with those of $^{A+1}Ba^+$ ($^{A+2}Ba^+$) ions (the superscripts A, A + 1, and A + 2 give the mass number of the Ba isotopes). Moreover, the reduced-mass change between different isotopomers of BaH^+ (BaD^+) is too small for a noticeable wavenumber shift between the corresponding R2PI spectra to be observable at the spectral resolution of our measurements.

To record PFI-ZEKE-PE spectra, electric-field pulse sequences were applied to the electrode stack, consisting of a first pulse of positive polarity to sweep prompt electrons out of the photoexcitation volume, followed by multiple pulses of negative polarity to field ionise high Rydberg states lying just below the ionisation thresholds. A sequence of seven electric-field pulses [(+0.09, −0.09, −0.17, −0.26, −0.34, −0.43, −1.72) V cm^{-1}] was employed to record high-resolution PFI-ZEKE-PE spectra following the procedure outlined in ref. 58 and 59. The photoelectrons released by the successive negative pulses of this sequence were extracted down the TOF tube and detected at the MCP detector in separate time-of-flight windows. Spectra were measured by monitoring the field-ionisation signals induced by each of the negative-field pulses of the sequence as a function of the wavenumber $\tilde{\nu}_2$ of the second laser. The shifts of the ionisation thresholds induced by the electric-field pulses were determined from PFI-ZEKE-PE spectra of the Ba(6s6p) $^1P_1$ → Ba^+(6s) $^2S_{1/2}$ photoionising transition recorded with the same electric-field pulse sequence. The differences between the observed line positions and the precisely known field-free ionisation threshold of Ba[60,61] were then used to correct for the field-induced shifts, resulting in an expected absolute accuracy of better than 0.2 cm^{-1} in the determination of the ionisation thresholds of BaH and BaD.

3. Results

3.1. (1 + 1′) R2PI spectra of the E $^2\Pi_{1/2}$ ($v' = 0, 1$) ← X $^2\Sigma^+$ ($v'' = 0$) transitions of BaH and BaD

In order to confirm the production of BaH/BaD as well as to characterise the rotational temperature of the BaH/BaD samples in the gas expansion, (1 + 1′) R2PI spectra of the E $^2\Pi_{1/2}$ ($v' = 1$, 0)–X $^2\Sigma^+$ ($v'' = 0$) bands were recorded. These bands were chosen because their rotational structure had been previously characterised at high-resolution by Ram *et al.* for BaH[35] and by Bernard *et al.* for BaD.[33] The E $^2\Pi_\Omega$ state also offered the advantage of having good Franck–Condon factors to the low-lying vibrational levels of the ionic X^+ $^1\Sigma^+$ ground state, allowing efficient ionisation.

The (1 + 1′) R2PI spectra for $^{134-138}BaH^+$ and $^{134-138}BaD^+$ were recorded after fixing the wavenumber $\tilde{\nu}_2$ of the ionisation

laser to 26 878.72 cm^{-1} and 25 400.00 cm^{-1}, respectively, well above the adiabatic ionisation thresholds of BaH and BaD, respectively. Attempts to record the R2PI spectra of bands involving higher vibrational levels of the E $^2\Pi_{1/2}$ and X $^2\Sigma^+$ states proved unsuccessful, reflecting the efficient cooling of the vibrational motion of BaH and BaD in the gas expansions and the diagonal nature of the E $^2\Pi_{1/2}$ (v')–X $^2\Sigma^+$ (v'') transitions.

Fig. 3 and 4 show as examples the R2PI spectrum of the E $^2\Pi_{1/2}$ (v' = 0)–X $^2\Sigma^+$ (v'' = 0) bands of ^{138}BaH and ^{138}BaD, respectively. The rotational structures of the BaH and BaD E $^2\Pi_{1/2}$ (v' = 1, 0)–X $^2\Sigma^+$ (v'' = 0) bands were analysed by fitting the molecular constants of effective Hamiltonians for $^2\Sigma^+$ and $^2\Pi$ states[62,63] to the observed rovibronic line positions. In this analysis, the E $^2\Pi_{1/2}$ state was treated as being intermediate between Hund's case (a) and (b) angular-momentum coupling cases while the X $^2\Sigma^+$ state was treated in pure Hund's case (b). To obtain the spectra displayed in orange colour in Fig. 3 and 4, the calculated stick spectra were convoluted with a Gaussian lineshape function with a full width at half maximum of 0.25 cm^{-1}. Rotational lines are labelled using the notation $^{\Delta N}\Delta J_{F_1(F_2)}(J'')$, where $\Delta N = N' - N''$, and F_1 and F_2 designate the spin–orbit (spin-rotational) components. In the X $^2\Sigma^+$ state, the F_1 and F_2 labels refer to the spin-rotational components with $J = N + 1/2$ and $J = N - 1/2$, respectively.[64] The $^2\Pi_{1/2}$ and $^2\Pi_{3/2}$ spin–orbit components of the E intermediate state are well separated and the rotational levels of the E $^2\Pi_{1/2}$ ($^2\Pi_{3/2}$) state are $F_1(F_2)$ levels, as expected for a $^2\Pi$ state with a positive spin–orbit-coupling constant in Hund's case (a) coupling. Accordingly, we use the subscripts "12" and "1" to label transitions that originate in X $^2\Sigma^+$ F_2 and F_1 levels, respectively. The experimental spectra are best reproduced with rotational temperatures T_{rot} of 12 K in the case of BaH and 8 K in the case of BaD, indicating a more efficient cooling of the rotational motion in BaD.

Table 1 lists the rotational B'_v and lambda-doubling p'_v constants obtained in the least-squares fit of the rotational

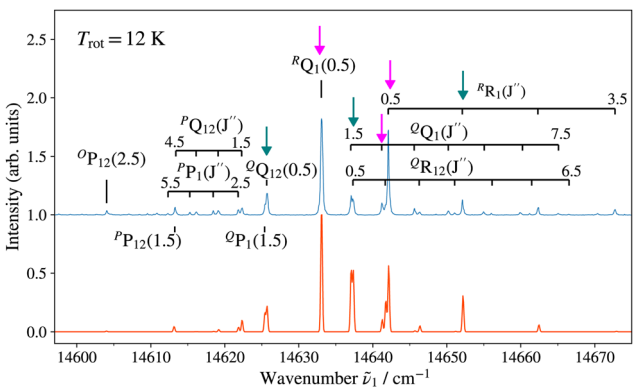

Fig. 3 (1 + 1′) R2PI spectrum of the E $^2\Pi_{1/2}$ (v' = 0)–X $^2\Sigma^+$ (v'' = 0) transition of ^{138}BaH acquired with an ionisation-laser wavenumber $\tilde{\nu}_2$ of 26 878.72 cm^{-1} with assignment of the highest-intensity $^{\Delta N}\Delta J_{F_1(F_2)}$ lines. Bottom: Spectrum calculated for a rotational temperature of 12 K and convoluted with a Gaussian lineshape function with a full width at half maximum of 0.25 cm^{-1}. The lines marked by vertical arrows (pink, aqua) are those used to prepare intermediate states of well-defined parity (−, +) to characterise the photoionisation dynamics.

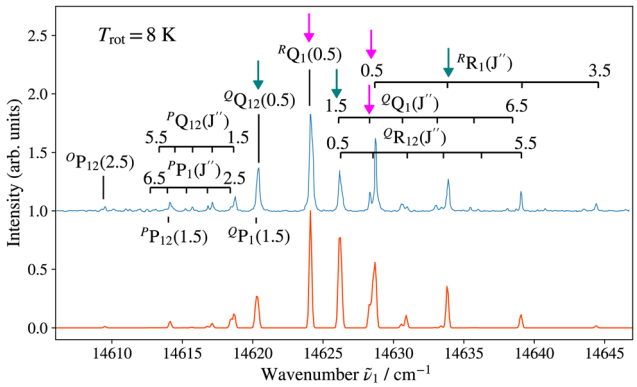

Fig. 4 (1 + 1′) R2PI spectrum of the E $^2\Pi_{1/2}$ (v' = 0)–X $^2\Sigma^+$ (v'' = 0) transition of ^{138}BaD acquired with an ionisation-laser wavenumber of $\tilde{\nu}_2$ of 25 400.00 cm^{-1} with assignment of the highest-intensity $^{\Delta N}\Delta J_{F_1(F_2)}$ lines. Bottom: Spectrum calculated for a rotational temperature of 8 K and convoluted with a Gaussian lineshape function with a full width at half maximum of 0.25 cm^{-1}. The lines marked by vertical arrows (pink, aqua) are those used to prepare intermediate states of well-defined parity (−, +) to characterise the photoionisation dynamics.

structure of the E $^2\Pi_{1/2}$ (v' = 1, 0)–X $^2\Sigma^+$ (v'' = 0) bands of ^{138}BaH and ^{138}BaD. It also provides the term values of the E $^2\Pi_{1/2}$ (v', N' = 1, J' = 0.5) rotational levels, corresponding to the position of the $^RQ_1(0.5)$ lines. The numbers in parentheses represent one standard deviation in units of the last digit. Overall, the results of our analysis are consistent with, though less precise than, the earlier results reported in ref. 33 and 35 with maximal deviations of about two standard deviations, *i.e.*, about 0.006 cm^{-1}. The rotational and lambda-doubling constants of the BaD E $^2\Pi_{1/2}$ (v' = 1) level are reported here for the first time.

3.2. PFI-ZEKE-PE spectra and characterisation of the X$^+$ $^1\Sigma^+$ ground state of BaH$^+$ and BaD$^+$

The photoionisation and PFI-ZEKE photoelectron spectra of ^{138}BaH in the vicinity of the ^{138}BaH$^+$ (v^+ = 0) ionisation threshold recorded from the intermediate E $^2\Pi_{1/2}$ (v' = 0, N' = 1, J' = 1.5, −) level of BaH are compared in Fig. 5. The photoionisation signal (Fig. 5a) gradually rises from a value of zero below ≈36 670 cm^{-1} to an approximately constant value above 36 725 cm^{-1} (full red line), reflecting contributions from successive ionisation continua associated with X$^+$ (v^+ = 0, N^+) states of increasing rotational quantum number N^+. It also exhibits sharp structures originating from the autoionisation of Rydberg states belonging to series converging on higher-lying rovibrational levels of BaH$^+$.

The BaH$^+$ rotational structure is fully resolved in the PFI-ZEKE-PE spectrum, as indicated by the assignment bar in Fig. 5b. Consequently, the adiabatic ionisation threshold $E_I/(hc)$ of ^{138}BaH, corresponding to the energy difference between the X$^+$ $^1\Sigma^+$ (v^+ = 0, N^+ = 0) and X $^2\Sigma^+$ (v'' = 0, N'' = 0, J'' = 0.5) ground states can be determined to be 38 679.96(20) cm^{-1}, the 0.2 cm^{-1} uncertainty originating primarily from the correction of the field-induced shift of the ionisation thresholds.

An overview of the rovibrational level structure of the X$^+$ $^1\Sigma^+$ electronic ground states of BaH$^+$ and BaD$^+$ as measured by PFI-ZEKE-PE spectroscopy following (1 + 1′) two-photon excitation

Table 1 Results of the rotational analysis of the (1 + 1′) R2PI spectra of the E $^2\Pi_{1/2}$ (v' = 1, 0)–X $^2\Sigma^+$ (v'' = 0) transitions of ^{138}BaH and ^{138}BaD. In the least-squares fits of the molecular constants, the values of the ground-state rotational constants B_0'' and γ_0'' of X $^2\Sigma^+$ ^{138}BaH and ^{138}BaD were fixed to the values reported by Ram *et al.*[35] and Birk *et al.*,[65] respectively. All values in cm^{-1}

	$Ev'/(hc)$ (N' = 1, J' = 0.5)	B_v'	p_v'	Ref.
BaH				
E $^2\Pi_{1/2}$ (v' = 0)	14 633.07(3)	3.480(3)	0.870(3)	This work
	14 633.0983[a]	3.4868233(40)	0.872460(93)	35
		3.48490(11)	0.87218(35)	33
E $^2\Pi_{1/2}$ (v' = 1)	15 819.42(3)	3.407(3)	0.882(3)	This work
	15 819.4909[a]	3.414457(14)	0.88520(24)	35
BaD				
E $^2\Pi_{1/2}$ (v' = 0)	14 624.13(3)	1.763(3)	0.433(3)	This work
		1.763230(33)	0.43251(29)	33
E $^2\Pi_{1/2}$ (v' = 1)	15 474.53(3)	1.730(3)	0.460(3)	This work

[a] Transitions end on the *e*-parity component of the E $^2\Pi_{1/2}$ (v', N' = 1, J' = 0.5) level.[35]

is presented in Fig. 6. The wavenumber scale in the figure is relative to the X $^2\Sigma^+$ (v'' = 0, N'' = 0, J'' = 0.5) ground states of BaH and BaD. The PFI-ZEKE-PE spectra display regular progressions of vibrational levels with v^+ = 0–5 for BaH$^+$ and v^+ = 0–4 for BaD$^+$. To observe these levels, it was necessary to use both the E $^2\Pi_{1/2}$ (v' = 0 and 1) intermediate levels, as indicated by the legend and the colour code in the figure (see also the second column of Table 2). Consequently, the relative intensities of the different bands cannot be directly compared.

To confirm the vibrational assignment of the PFI-ZEKE-PE spectra, a standard isotopic-shift analysis[66] was performed. The isotopic shifts expected for the lowest five observed vibrational levels of the X$^+$ $^1\Sigma^+$ state were determined using the vibrational constants of the BaH X $^2\Sigma^+$ and BaH$^+$ X$^+$ $^1\Sigma^+$ states reported by Ram *et al.*[35] and in the present work, respectively. They are

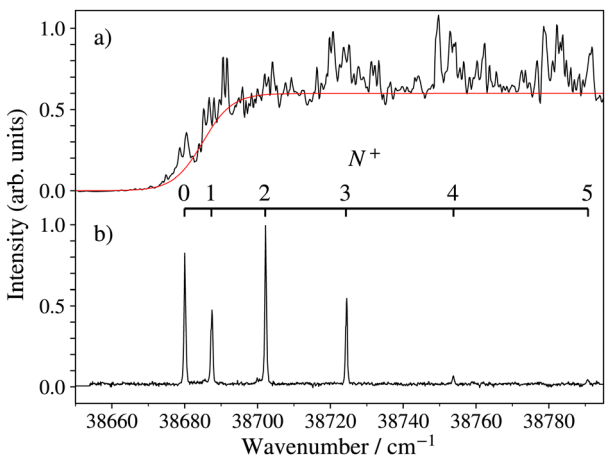

Fig. 5 Photoionisation (a) and PFI-ZEKE-photoelectron (b) spectra of ^{138}BaH in the vicinity of the BaH$^+$ X$^+$ $^1\Sigma^+$ (v^+ = 0) ionisation threshold and recorded from the BaH E $^2\Pi_{1/2}$ (v' = 0, N' = 1, J' = 1.5, −) intermediate level. The PFI-ZEKE-PE spectrum has been corrected for the field-induced shift of the ionisation thresholds. The wavenumber scale is with respect to the X $^2\Sigma^+$ (v'' = 0, N'' = 0) ground state of BaH.

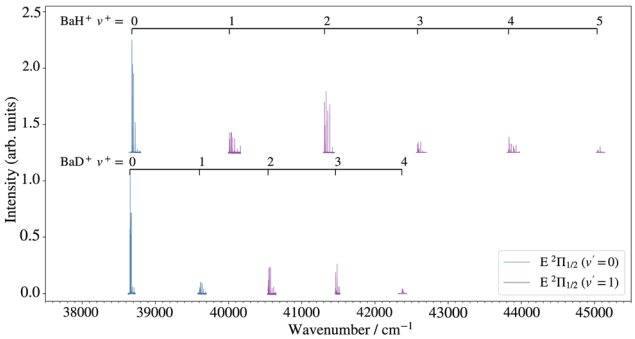

Fig. 6 Overview of the rovibrational energy-level structure of the BaH$^+$ and BaD$^+$ X$^+$ $^1\Sigma^+$ states obtained by PFI-ZEKE-PE spectroscopy following resonant two-photon excitation from the X $^2\Sigma^+$ ground state of BaH/BaD *via* the E $^2\Pi_{1/2}$ (v' = 0, 1) levels, as indicated by the colour code and the legends.

displayed in Fig. 7 as dashed and thick lines, corresponding to vibrational assignments of v^+ = 0–4 and v^+ = 1–5 for the observed bands, respectively. The experimentally observed isotopic shifts (blue dots in Fig. 7) enable the unambiguous assignment of the lowest observed levels to the v^+ = 0 ground levels of BaH$^+$ and BaD$^+$, which is consistent with the onset of the photoionisation signal (see Fig. 5a).

Table 2 lists, in the third column, the positions of the field-free X$^+$(v^+, N^+ = 0) ionisation thresholds of BaH and BaD relative to the respective X (v'' = 0, N'' = 0) neutral ground states derived from the PFI-ZEKE photoelectron spectra. The uncertainties in these thresholds are purely statistical and do not include a systematic contribution of 0.2 cm^{-1} originating from the uncertainty in the determination of the shifts of the ionisation thresholds induced by the pulsed electric fields (see Section 2). These shifts are expected to be the same for all ionisation thresholds and, therefore, the systematic uncertainties cancel out when determining the vibrational term values T_{v^+} given in the fifth column. The adiabatic ionisation wavenumbers of ^{138}BaH and ^{138}BaD, corresponding to the X$^+$ $^1\Sigma^+$ (v^+ = 0, N^+ = 0) ← X $^2\Sigma^+$ (v'' = 0, N'' = 0) ionising transition, are thus 38 679.96(20) cm^{-1} [4.79570(3) eV] and 38 652.69(20) cm^{-1} [4.79232(3) eV], respectively. The value for BaH lies ≈1070 cm^{-1} above the value of 37 607 cm^{-1} predicted by dos Santos *et al.*[40] Table 2 also gives, in the fourth column, the ionic vibrational term values and, in the fifth column, the residuals ($\tilde{\nu}_{calc} - \tilde{\nu}_{exp}$) obtained in a least-squares fit of the harmonic (ω_e) and anharmonic ($\omega_e x_e$, $\omega_e y_e$) vibrational constants. The fitted values of these constants are listed in Table 3 below.

The PFI-ZEKE photoelectron spectra recorded from selected rotational levels [N', J', (−/+)] of the intermediate E $^2\Pi_{1/2}$ (v' = 0, 1) states are rotationally fully resolved and the left- and right-hand-side panels of Fig. 8 show, as representative examples, the spectra of the X$^+$ $^1\Sigma^+$ (v^+ = 0, N^+) ← E $^2\Pi_{1/2}$ [v' = 0, J' = 1.5, 2.5, (−/+)] ionising transitions of BaH and BaD, respectively.

A striking feature of these PFI-ZEKE PE spectra is the intensity alternation of transitions to successive rotational levels (N^+) of the cations. Transitions to BaH$^+$/BaD$^+$ levels of even (odd) N^+ values are found to be dominant when ionisation occurs from rotational levels of the intermediate state of

Table 2 Ionisation thresholds $E_{v^+}/(hc)$ corresponding to the positions of the vibrational levels of the $X^+\ ^1\Sigma^+$ ground state of $^{138}BaH^+$ and $^{138}BaD^+$ (in cm^{-1}) with respect to the respective $X\ ^2\Sigma^+$ (v'' = 0, N'' = 0) ground state of BaH or BaD, obtained following (1 + 1′) resonant two-photon excitation from the $X\ ^2\Sigma^+$ (v'' = 0) level of BaH and BaD *via* the $E\ ^2\Pi_{1/2}$ (v' = 0, 1) levels, as listed in the second column. Vibrational term values T_{v^+} and rotational constants B_{v^+} determined from least-squares fit to the rotational structure of the PFI-ZEKE-PE spectra are given (in cm^{-1}) in the last two columns. $\tilde{\nu}_{calc} - \tilde{\nu}_{exp}$ are the residuals of the fits of the threshold positions to polynomial expansions in $v^+ + 1/2$ used to determine the values of ω_e, $\omega_e x_e$ and $\omega_e y_e$ listed in Table 3

v^+	$^{2S+1}\Lambda'_{\Omega'}$ (v')	$E_{v^+}/(hc)$[a]; (N^+ = 0)	$\tilde{\nu}_{calc} - \tilde{\nu}_{exp}$	T_{v^+}	B_{v^+}
BaH^+					
0	$E\ ^2\Pi_{1/2}$ (0)	38 679.96(3)	0.006	0.0	3.6835(18)
1	$E\ ^2\Pi_{1/2}$ (1)	40 010.55(4)	−0.025	1330.59(5)	3.6255(18)
2	$E\ ^2\Pi_{1/2}$ (1)	41 311.81(3)	0.036	2631.85(4)	3.5650(16)
3	$E\ ^2\Pi_{1/2}$ (1)	42 583.25(3)	−0.022	3903.29(4)	3.4973(15)
4	$E\ ^2\Pi_{1/2}$ (1)	43 824.72(3)	0.004	5144.76(4)	3.4332(16)
5	$E\ ^2\Pi_{1/2}$ (1)	45 035.61(4)	0.001	6355.65(5)	3.3647(23)
BaD^+					
0	$E\ ^2\Pi_{1/2}$ (0)	38 652.69(3)	−0.002	0.0	1.8645(4)
1	$E\ ^2\Pi_{1/2}$ (0)	39 603.59(3)	−0.013	950.90(4)	1.8462(13)
2	$E\ ^2\Pi_{1/2}$ (1)	40 539.696(22)	0.048	1887.01(4)	1.8195(8)
3	$E\ ^2\Pi_{1/2}$ (1)	41 461.09(3)	−0.051	2808.40(4)	1.7971(16)
4	$E\ ^2\Pi_{1/2}$ (1)	42 367.46(4)	0.018	3714.77(5)	1.784(3)

[a] The uncertainties correspond to one standard deviation and do not include a 0.2 cm^{-1} systematic uncertainty arising from the compensation of the field-induced shift of the ionisation thresholds.

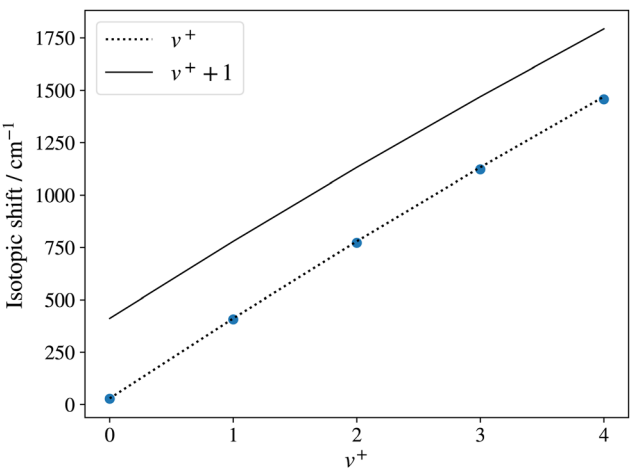

Fig. 7 Isotopic shift of the v^+ = 0–4 levels of $^{138}BaD^+$ with respect to those of $^{138}BaH^+$ determined from PFI-ZEKE-PE spectra of the $X^+\ ^1\Sigma^+$ (v^+) ← $E\ ^2\Pi_{1/2}$ (v' = 1, 0) photoionising transitions. The dotted and full lines are the predictions for the cases where the lowest observed level corresponds to v^+ = 0 and v^+ = 1, respectively. The shifts were calculated from the molecular constants reported by Ram *et al.*[35] for the BaH $X\ ^2\Sigma^+$ state and those determined in the present work for the $BaH^+\ X^+\ ^1\Sigma^+$ state.

positive (negative) parity, as illustrated schematically in Fig. 9 for the BaH $X^+\ ^1\Sigma^+$ (v^+, N^+) ← $E\ ^2\Pi_{1/2}$ (v', J' = 1.5) ionising transitions.

Single-photon excitation is accompanied by a change of the rovibronic parity ($\pm \leftrightarrow \mp$). In a photoionisation transition, the parity of the final state is a product of the rovibronic parity of the ionised molecule [here, $p_{ion} = (-1)^{N^+}$] and the parity of the photoelectron partial wave $(-1)^{\ell'}$. Consequently, the rovibrational parity selection rule for a transition from a rovibronic state of the parent neutral molecule with parity $p_{neutral}$ can be expressed as (ref. 67)

$$p_{ion} = (-1)^{\ell'+1} p_{neutral}. \quad (1)$$

The experimentally observed intensity alternations indicate a preponderance of transitions connecting rovibronic levels of opposite parity, *i.e.*, associated with the emission of even-ℓ' photoelectron partial waves or, in the case of the high Rydberg states detected by PFI-ZEKE-PE spectroscopy, of Rydberg states accessed optically through their even-ℓ' character. In a simple "orbital-ionisation" model,[68–70] this preponderance can be interpreted as a dominant odd-ℓ character of the molecular orbital of the $E\ ^2\Pi_{1/2}$-state principal electronic configuration out of which the electron is ejected.

In this model, the relative photoionisation cross section is expressed as a superposition of contributions from different orbital-angular-momentum (ℓ) components in a single-centre expansion of the outermost valence orbital of the intermediate state[68,70]

$$\sigma_{tot} \propto \sum_{\ell=\lambda}^{\ell_{max}} \frac{1}{2\ell+1} Q(\ell) C_\ell. \quad (2)$$

In eqn (2), λ corresponds to the projection of $\vec{\ell}$ on the molecular axis and C_ℓ are adjustable coefficients, as explained in ref. 71. The geometric factor

$$Q(\ell) = (2N^+ + 1) \sum_\chi (2\chi + 1) \begin{pmatrix} \ell & S' & \chi \\ \lambda & \Sigma' & \Lambda^+ - \Omega' \end{pmatrix}^2 \begin{pmatrix} N^+ & \chi & J' \\ -\Lambda^+ & \Lambda^+ - \Omega' & \Omega' \end{pmatrix}^2 \quad (3)$$

describes the relative rotational intensities for a photoionisation transition from an intermediate level of $^2\Pi$ symmetry [Hund's case (a)] to an ionic level of $^1\Sigma^+$ symmetry [Hund's case (b)]. As eqn (3) does not inherently distinguish between ionisation processes occurring from rotational levels of different parity, the parity selection rule (eqn (1)) must be enforced in the calculation of $Q(\ell)$ for ionisation to individual N^+ levels of the ion from rotational levels of the intermediate $E\ ^2\Pi_{1/2}$ state of specific parity.

Satisfactory agreement with the measured intensities could be reached by retaining only single-centre expansion components of low ℓ values, and the model calculations presented in blue and red in Fig. 8 assume, for simplicity, that only ℓ = 1 and ℓ = 2 are needed to generate the even- and odd-ℓ' partial waves, in a ratio of 1 : 0.55. While the calculations account for the main trends of the observed intensity distributions, discrepancies remain. In particular, transitions with negative values of N^+–J' are typically stronger than those of the corresponding positive N^+–J' values. This behaviour is observed in many other molecules and can be attributed to rotational channel interactions, as explained in detail in ref. 71. Moreover, transitions to the

Table 3 Comparison of the molecular constants of $^{138}BaH^+$ and $^{138}BaD^+$ derived in this work with selected literature values. All values in cm^{-1}

	$T_0/(hc)$	ω_e	$\omega_e x_e$	$\omega_e y_e$	B_e	α_e	γ_e	r_e (Å)	Ref.
BaH^+ X^+ $^1\Sigma^+$	38 679.96(3)[a]	1359.65(10)	14.43(4)	−0.058(4)	3.7128(21)	0.0568(16)	−0.0012(3)	2.1273(8)	This work
	37 607	1394						2.089	40
		1352.7			3.711	0.060		2.139	41
		1370	15		3.623	0.067		2.156	17
BaD^+ X^+ $^1\Sigma^+$	38 652.69(3)[a]	965.84(7)	7.429(13)		1.875(4)	0.0210(13)		2.1284(20)	This work
		960			1.870	0.021		2.139	41[b]
		973	7.6		1.827	0.024		2.156	17[b]

[a] With respect to the $X\ ^2\Sigma^+$ ($v'' = 0$, $N'' = 0$) ground states of $^{138}BaH/^{138}BaD$. The uncertainty does not include a systematic contribution of 0.2 cm^{-1} originating from the correction of the field-induced shift of the ionisation thresholds. [b] Molecular constants of ^{138}BaH as reported in ref. 17 and 41 multiplied by the reduced mass ratio $(\mu_{BaH}/\mu_{BaD})^{i/2+j}$, where i and j represent the exponents of $v^+ + 1/2$ and $N^+(N^+ + 1)$ in the corresponding terms of the standard expressions for the rovibrational term values,[66] respectively.

$N^+ = 5$, − ionic level associated with odd-ℓ' partial waves in the spectra recorded from the $J' = 2.5$, − levels of both BaH and BaD (bottom panels of Fig. 8) are weaker than predicted by the calculations (see red traces). This observation may reflect a mixing of $^2\Pi_{1/2}$ and $^2\Sigma_{1/2}{}^+$ character in the E $^2\Pi_{1/2}$ state induced by the spin–orbit interaction,[64] which would allow an $\ell = 0$ contribution in the single-centre expansion of the molecular-orbital and enhance the relative intensity of the transition to the $N^+ = 1$ and 3 levels compared to that to the $N^+ = 5$ level in the calculated spectrum. Alternatively, the intensity of these

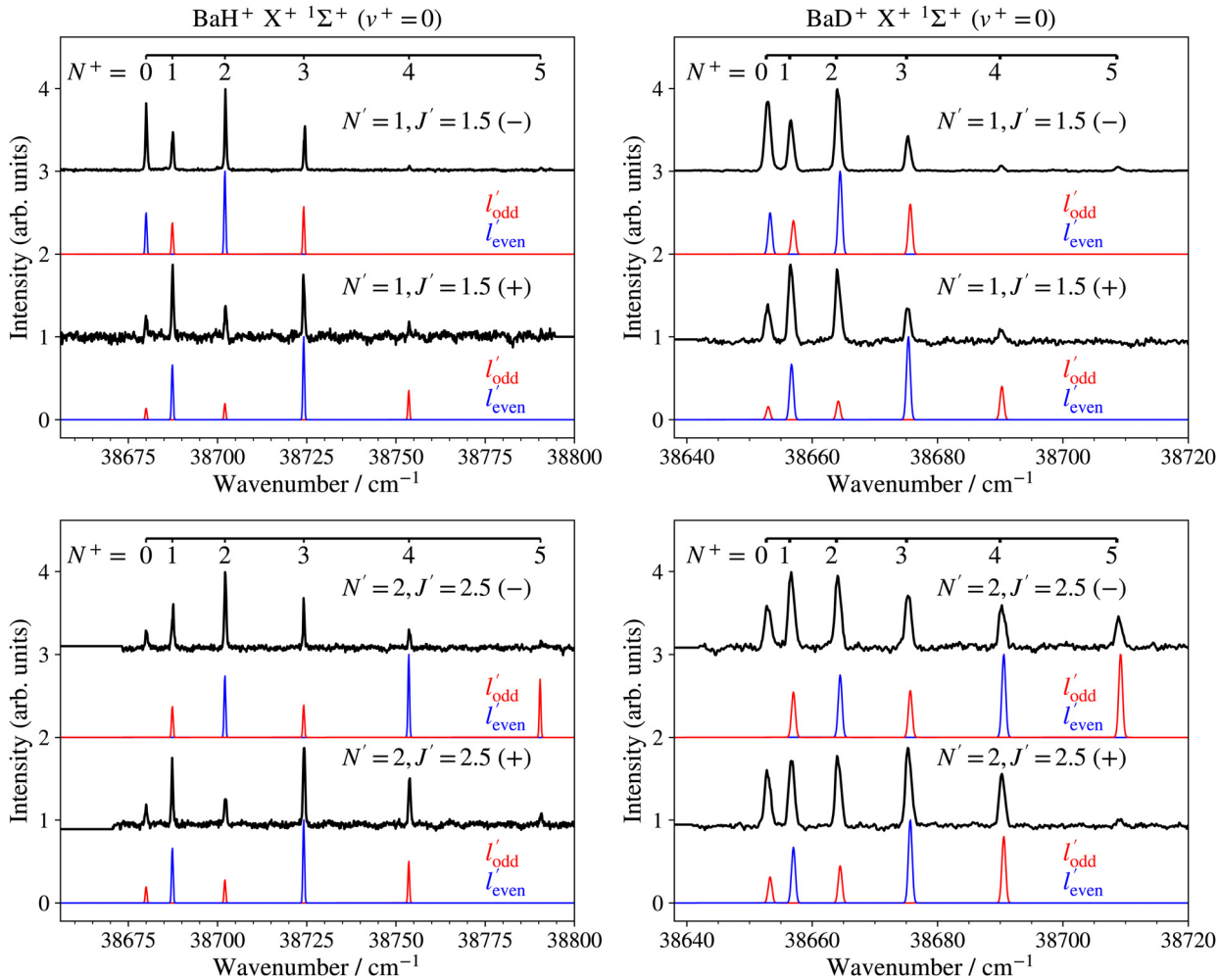

Fig. 8 High-resolution PFI-ZEKE-PE spectra of the $X^+\ ^1\Sigma^+$ ($v^+ = 0$, N^+) ← E $^2\Pi_{1/2}$ [$v' = 0$, N', J', (−/+)] ionising transitions of BaH and BaD. The assignment bars give the values of the rotational quantum N^+. The blue and red traces correspond to intensity contributions from different configurations of the E $^2\Pi_{1/2}$ state and expected for ionisation out of molecular orbitals of dominant $\ell = 1$ (ℓ' even) and 2 (ℓ' odd) chararacters, respectively, in single-centre expansions of the orbitals.

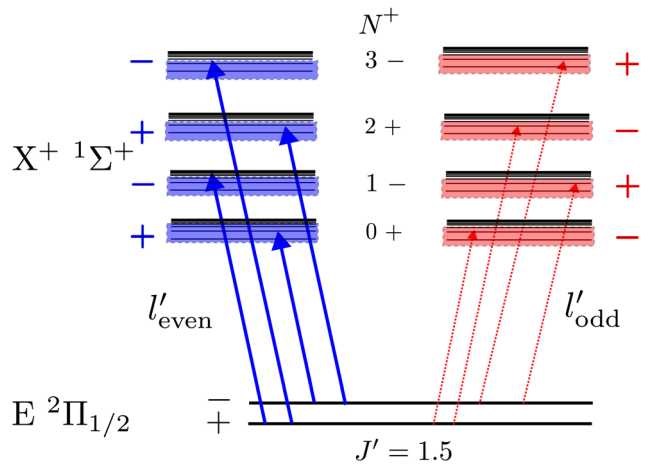

Fig. 9 Illustration of rovibronic photoionisation parity selection rules observed in transitions from the J = 1.5, p_{neutral} = ± rotational levels of the E $^2\Pi_{1/2}$ state of BaH and BaD to the N^+ = 0–3, $p_{\text{ion}} = (-1)^{N+}$ rotational levels of the X$^+$ $^1\Sigma^+$ state of BaH$^+$ and BaD$^+$. See text for details.

transitions could be reduced by destructive partial-wave interferences, which are not treated in the model.

The rotational constants of the X$^+$ $^1\Sigma^+$ (v^+) levels were determined from the experimental line positions in a least-squares fit based on a Hund's case (b) energy expression.[66] Their values are listed in the fifth column of Table 2. Because we only observed rotational levels with $N^+ \leq 5$, the experimental term values could be accounted for within the experimental uncertainties (weighted RMS deviations of 0.265 (BaH) and 0.254 (BaD)) without considering centrifugal distortion effects.

Table 3 presents the equilibrium molecular constants ω_e, $\omega_e x_e$, $\omega_e y_e$, B_e, α_e, and γ_e of the X$^+$ $^1\Sigma^+$ ground states of BaH$^+$ and BaD$^+$ extracted from analyses based on the standard power-series expansions in $v^+ + 1/2$ and $N^+(N^+ + 1)$.[66] To reach a satisfactory description of the rovibrational structure, it was necessary to include anharmonicity terms up to the third order ($\omega_e y_e$) in BaH$^+$ and second order ($\omega_e x_e$) in BaD$^+$, as well as up to second-order corrections to the rotational constant [$B_v = B_e - \alpha_e(v + 1/2) + \gamma_e(v + 1/2)^2$]. The molecular equilibrium constants in Table 3 for BaH$^+$ are in best agreement with the *ab initio* calculations by Allouche *et al.*[17] and Abe *et al.*[41] In the case of BaD$^+$, we compare the molecular constants derived from the PFI-ZEKE-PE spectra with values derived from the ^{138}BaH$^+$ molecular constants reported in ref. 17 and 41 using the appropriate scaling with the reduced-mass ratio, *i.e.*, $(\mu_{\text{BaH}}/\mu_{\text{BaD}})^{i/2+j}$, where i and j are the exponents of $v^+ + 1/2$ and $N^+(N^+ + 1)$ in the corresponding terms of the standard expressions for the rovibrational term values,[66] respectively. These values are reported in Table 3 and are in good agreement with the values extracted from our spectra.

Table 4 Lowest pure-rotational transition frequencies in the X$^+$ $^1\Sigma^+$ (v^+ = 0) ground states of BaH$^+$ and BaD$^+$, as determined from the analysis of the PFI-ZEKE-PE spectra. The uncertainties include a contribution from possible centrifugal-distortion effects not included in the analysis of the rotational structure

	(J'–J'')	ν (GHz)
BaH$^+$	(1–0)	220.86(11)
	(2–1)	441.71(11)
	(3–2)	662.57(11)
BaD$^+$	(1–0)	111.79(3)
	(2–1)	223.59(3)
	(3–2)	335.38(3)

4. Conclusions

We have presented an experimental investigation of the rovibronic photoionisation dynamics of BaH and BaD and of the rovibrational structures of the X$^+$ $^1\Sigma^+$ ground electronic states of BaH$^+$ and BaD$^+$. From the fully resolved rotational structure of photoelectron spectra of BaH and BaD recorded following resonant (1 + 1′) two-photon excitation from the ground neutral state *via* selected rovibrational levels of the intermediate E $^2\Pi_{1/2}$ state, we could derive rovibrational molecular constants for the X$^+$ $^1\Sigma^+$ ground electronic states of BaH$^+$ and BaD$^+$ and determine precise values of the adiabatic ionisation energies of BaH and BaD, as summarised in Tables 2 and 3.

The rotational intensity distributions in the photoelectron spectra recorded from E $^2\Pi_{1/2}$-state rotational levels of selected parity exhibit marked intensity differences between transitions to ionic rotational levels of even and odd values of the rotational quantum number N^+, revealing dominant contributions from even-ℓ' photoelectron partial waves. These observations were interpreted in terms of mixed configurations of the E $^2\Pi_{1/2}$ state in the realm of a simple single-centre orbital-ionisation model, revealing overall satisfactory agreement, but also pronounced discrepancies for transitions associated with odd-ℓ' partial waves and angular-momentum transfer N^+–J' of + 2.5. These discrepancies call for a more refined treatment of the rovibrational photoionisation dynamics of BaH and BaD.

Pure rotational transitions have not been observed yet in BaH$^+$ and BaD$^+$ but would be needed for a more precise characterisation of their structure and for radio-astronomical searches for these ions, in particular near sunspots where the parent neutral molecules have been predicted to occur but have not been detected yet despite recent efforts.[72] Table 4 lists the transition frequencies of the lowest pure-rotational transitions of BaH$^+$ and BaD$^+$ derived from the analysis of the PFI-ZEKE photoelectron spectra, which may be helpful for future laboratory measurements and astrophysical searches.

Data availability

All data are presented in the article. They can be obtained from the authors upon reasonable request.

Conflicts of interest

There are no conflicts of interest to declare.

Acknowledgements

We thank Josef A. Agner and Hansjürg Schmutz for their technical assistance and Carla Kreis for discussions. This work is supported financially by the Swiss National Science Foundation (grant No. 200020B-200478).

References

1 H. Wöhl, *Sol. Phys.*, 1971, **16**, 362–372.
2 J. D. Kirkpatrick, *Annu. Rev. Astron. Astrophys.*, 2005, **43**, 195–245.
3 H.-I. Lu, J. Rasmussen, M. J. Wright, D. Patterson and J. M. Doyle, *Phys. Chem. Chem. Phys.*, 2011, **13**, 18986–18990.
4 R. L. McNally, I. Kozyryev, S. Vazquez-Carson, K. Wenz, T. Wang and T. Zelevinsky, *New J. Phys.*, 2020, **22**, 083047.
5 S. Vázquez-Carson, Q. Sun, J. Dai, D. Mitra and T. Zelevinsky, *New J. Phys.*, 2022, **24**, 083006.
6 K. Gaul, S. Marquardt, T. Isaev and R. Berger, *Phys. Rev. A*, 2019, **99**, 032509.
7 D. Segal, V. Lorent, R. Dubessy and B. Darquié, *J. Mod. Opt.*, 2018, **65**, 490–500.
8 N. M. Fazil, V. S. Prasannaa, K. V. P. Latha, M. Abe and B. P. Das, *Phys. Rev. A*, 2019, **99**, 052502.
9 M. Kajita and Y. Moriwaki, *J. Phys. B: At., Mol. Opt. Phys.*, 2009, **42**, 154022.
10 K. Højbjerre, A. K. Hansen, P. S. Skyt, P. F. Staanum and M. Drewsen, *New J. Phys.*, 2009, **11**, 055026.
11 A. T. Calvin, S. Janardan, J. Condoluci, R. Rugango, E. Pretzsch, G. Shu and K. R. Brown, *J. Phys. Chem. A*, 2018, **122**, 3177–3181.
12 S. A. Jones, *New J. Phys.*, 2022, **24**, 023016.
13 P. Fuentealba and O. Reyes, *Mol. Phys.*, 1987, **62**, 1291–1296.
14 W. Müller, J. Flesch and W. Meyer, *J. Chem. Phys.*, 1984, **80**, 3297–3310.
15 M. Kaupp, P. V. R. Schleyer, H. Stoll and H. Preuss, *J. Chem. Phys.*, 1991, **94**, 1360–1366.
16 A. R. Allouche, G. Nicolas, J. C. Barthelat and F. Spiegelmann, *J. Chem. Phys.*, 1992, **96**, 7646–7655.
17 A. R. Allouche, F. Spiegelmann and M. Aubert-Frécon, *Chem. Phys. Lett.*, 1993, **204**, 343–349.
18 K. Moore, B. M. McLaughlin and I. C. Lane, *J. Chem. Phys.*, 2016, **144**, 144314.
19 Y. Gao and T. Gao, *Phys. Rev. A: At., Mol., Opt. Phys.*, 2014, **90**, 052506.
20 G. Z. Iwata, R. L. McNally and T. Zelevinsky, *Phys. Rev. A*, 2017, **96**, 022509.
21 K. Moore and I. C. Lane, *J. Quant. Spectrosc. Radiat. Transfer*, 2018, **211**, 96–106.
22 A. Schaafsma, *Z. Phys.*, 1932, **74**, 254–266.
23 W. R. Fredrickson and W. W. Watson, *Phys. Rev.*, 1932, **39**, 753–764.
24 W. W. Watson, *Phys. Rev.*, 1933, **43**, 9–11.
25 W. W. Watson, *Phys. Rev.*, 1935, **47**, 213–214.
26 B. Grundström, *Z. Phys.*, 1936, **99**, 595–606.
27 M. Aslam Khan, *J. Phys. B: At. Mol. Phys.*, 1968, **1**, 985.
28 M. Aslam Baig, M. Rafi and M. Aslam Khan, *Il Nuovo Cimento B*, 1977, **40**, 365–370.
29 M. Rafi, S. Ahmed, M. Aslam Khan and M. Aslam Baig, *Z. Phys. A*, 1985, **320**, 369–373.
30 G. Fabre, A. E. Hachimi, R. Stringat, C. Effantin, A. Bernard, J. D'Incan and J. Verges, *J. Phys. B: At. Mol. Opt. Phys.*, 1987, **20**, 1933.
31 M. Rafi, A. Al-Ghamdi, K. Ahmed and I. Khan, *Phys. Lett. A*, 1994, **189**, 304–306.
32 O. Appelblad, L.-E. Berg, L. Klynning and J. W. C. Johns, *Phys. Scr.*, 1985, **31**, 69.
33 A. Bernard, C. Effantin, J. D'Incan, G. Fabre, R. Stringat and R. Barrow, *Mol. Phys.*, 1989, **67**, 1–18.
34 R. F. Barrow, B. J. Howard, A. Bernard and C. Effantin, *Mol. Phys.*, 1991, **72**, 971–976.
35 R. S. Ram and P. F. Bernath, *J. Mol. Spectrosc.*, 2013, **283**, 18–21.
36 U. Magg, H. Birk and H. Jones, *Chem. Phys. Lett.*, 1988, **149**, 321–325.
37 H. G. H. Kaley, A. Walker and P. F. Bernath, *Mol. Phys.*, 1993, **78**, 577–589.
38 M. G. Tarallo, G. Z. Iwata and T. Zelevinsky, *Phys. Rev. A*, 2016, **93**, 032509.
39 K. Moore, I. C. Lane, R. L. McNally and T. Zelevinsky, *Phys. Rev. A*, 2019, **100**, 022506.
40 L. G. dos Santos and F. R. Ornellas, *Chem. Phys.*, 2019, **520**, 32–39.
41 M. Abe, M. Kajita, M. Hada and Y. Moriwaki, *J. Phys. B: At., Mol. Opt. Phys.*, 2010, **43**, 245102.
42 L. Mejrissi, H. Habli, H. Ghalla, B. Oujia and F. X. Gadéa, *J. Phys. Chem. A*, 2013, **117**, 5503–5517.
43 N. Abu el kher, I. Zeid, N. El-Kork and M. Korek, *J. Comput. Sci.*, 2021, **51**, 101264.
44 M. Aymar and O. Dulieu, *J. Phys. B: At., Mol. Opt. Phys.*, 2012, **45**, 215103.
45 S. Falcinelli, F. Fernández-Alonso, K. S. Kalogerakis and R. N. Zare, *Mol. Phys.*, 1996, **88**, 663–672.
46 D. Schröder and H. Schwarz, *J. Phys. Chem. A*, 1999, **103**, 7385–7394.
47 S. Falcinelli and M. Rosi, *Molecules*, 2020, **25**, 4157.
48 D. Wehrli, M. Génévriez and F. Merkt, *Phys. Chem. Chem. Phys.*, 2021, **23**, 10978–10987.
49 G. Reiser, W. Habenicht, K. Müller-Dethlefs and E. W. Schlag, *Chem. Phys. Lett.*, 1988, **152**, 119–123.
50 K. Müller-Dethlefs and E. W. Schlag, *Ann. Rev. Phys. Chem.*, 1991, **42**, 109–136.
51 F. Merkt, S. Willitsch and U. Hollenstein, in *Handbook of High-Resolution Spectroscopy*, ed. M. Quack, F. Merkt, John Wiley & Sons, Chichester, 2011, vol. 3, pp. 1617–1654.
52 C. Kreis, M. Holdener, M. Génévriez and F. Merkt, *Mol. Phys.*, 2023, **121**, e2152746.
53 M. Génévriez, D. Wehrli and F. Merkt, *Mol. Phys.*, 2020, **118**, e1703051.
54 D. Wehrli, M. Génévriez, C. Kreis, J. A. Agner and F. Merkt, *J. Phys. Chem. A*, 2020, **124**, 379–385.
55 M. Génévriez, D. Wehrli, J. A. Agner and F. Merkt, *Int. J. Mass Spectrom.*, 2019, **435**, 209–216.

56 C. Kreis, J. R. Schmitz and F. Merkt, *Phys. Chem. Chem. Phys.*, 2024, **26**, 19359–19368.
57 M. Berglund and M. E. Wieser, *Pure Appl. Chem.*, 2011, **83**, 397–410.
58 S. Mollet and F. Merkt, *J. Chem. Phys.*, 2013, **139**, 034302.
59 J. R. Schmitz, U. Hollenstein and F. Merkt, *Mol. Phys.*, 2023, **121**, e2232888.
60 B. H. Post, W. Vassen, W. Hogervorst, M. Aymar and O. Robaux, *J. Phys. B: At. Mol. Phys.*, 1985, **18**, 187.
61 H. Karlsson and U. Litzén, *Phys. Scr.*, 1999, **60**, 321.
62 J. M. Brown and A. J. Merer, *J. Mol. Spectrosc.*, 1979, **74**, 488–494.
63 R. N. Zare, *Angular momentum: Understanding spatial aspects in chemistry and physics*, John Wiley & Sons, New York, 1988.
64 H. Lefebvre-Brion and R. W. Field, *The Spectra and Dynamics of Diatomic Molecules*, Elsevier, Amsterdam, 2004.
65 H. Birk, R. Urban, P. Polomsky and H. Jones, *J. Chem. Phys.*, 1991, **94**, 5435–5442.
66 G. Herzberg, *Molecular Spectra and Molecular Structure. Spectra of Diatomic Molecules*, Krieger, Malabar, 1989, vol. 1.
67 R. Signorell and F. Merkt, *J. Chem. Phys.*, 1998, **109**, 9762–9771.
68 A. D. Buckingham, B. J. Orr and J. M. Sichel, *Philos. Trans. R. Soc. London*, 1970, **268**, 147–157.
69 J. M. Sichel, *Mol. Phys.*, 1970, **18**, 95–100.
70 S. Willitsch and F. Merkt, *Int. J. Mass Spectrom.*, 2005, **245**, 14–25.
71 F. Merkt and T. P. Softley, *Int. Rev. Phys. Chem.*, 1993, **12**, 205–239.
72 B. Karthikeyan, G. Shanmugapriya, N. Rajamanickam and S. Bagare, *New Astron.*, 2020, **78**, 101366.